

Autoionizing decay of H_2 doubly excited states by using xuv-pump–infrared-probe schemes with trains of attosecond pulses

R. E. F. Silva,¹ P. Rivière,^{1,*} and F. Martín^{1,2}¹*Departamento de Química, Módulo 13, Universidad Autónoma de Madrid, 28049 Madrid, Spain*²*Instituto Madrileño de Estudios Avanzados en Nanociencia, Cantoblanco, 28049 Madrid, Spain*

(Received 24 April 2012; published 22 June 2012)

We present a theoretical study of H_2 ionization by a pump-probe scheme consisting on an attosecond pulse train (APT) and a near-infrared (IR) pulse. We focus on the autoionization dynamics of the first series of resonant states of the molecule, the Q_1 doubly excited states. The APT central frequency is tuned to populate the $^1\Sigma_u^+$ resonant states. The trace of autoionization is clearly visible in the two-dimensional (2D) proton-electron coincidence spectra and in the proton kinetic energy spectra. The dynamics of the autoionization process is clearly visible in the movie obtained by plotting the 2D spectrum as a function of the time delay between the APT and IR pulses. An analysis of the final symmetries Σ_g and Σ_u allows us to track the origin of the different structures.

DOI: [10.1103/PhysRevA.85.063414](https://doi.org/10.1103/PhysRevA.85.063414)

PACS number(s): 33.80.Eh, 33.20.Xx, 42.65.Re

I. INTRODUCTION

Ultrashort laser pulses are an excellent tool to study the dynamics of molecular photoionization. Combined with kinematically complete experiments, in which the momentum of all ejected electrons and atomic ions is determined in coincidence, they have made possible to obtain detailed information of the photoionization process [1–8]. These kinds of experiments open the door to unravel the dynamics of autoionization, a process triggered by electron correlation. Autoionization may occur when two or more valence electrons are excited and one of them is spontaneously ejected in the continuum, or when one inner-shell electron is missing, so an electron from an upper shell occupies the hole and another electron is ejected (Auger effect). This laser-assisted photoemission process is now widely used to track fast electron dynamics in atoms, and to characterize x-ray pulses [9–13].

In molecules, autoionization lifetimes are typically of the same order of magnitude as the molecular vibrational period or the time for molecular dissociation. Thus the nuclei have enough time to move outside the Franck-Condon (FC) region before the electron is ejected. Therefore, a correct theoretical description requires not only that electron correlation is well described, but also that nuclear motion is included. Furthermore, autoionization and direct ionization may interfere, so a fully quantum mechanical treatment of both nuclear and electronic motion is required. Hence describing autoionization in molecules is in general a formidable challenge.

For these reasons, a complete description of the autoionization process in molecules is only possible for the simplest molecular system, H_2 (or D_2), for which a theoretical method that fulfills the previous requirements has been recently proposed and adapted to treat autoionization [14–16]. This is the method that will be used in the present work. In the H_2 molecule, doubly excited states (DES) are embedded in and coupled to the electronic continuum through electron correlation [17,18], and can thus contribute to nondissociative ($H^{**} \rightarrow H_2^+ + e^-$) or dissociative ($H^{**} \rightarrow H + H^+ + e^-$)

ionization. The DES states can also dissociate into two neutral ($H + H$) or ionic ($H^+ + H^-$) fragments.

So far, single attosecond pulses (SAP) have been used to study autoionization in H_2 both in xuv-pump–xuv-probe setups [19] and in combination with IR fields [20]. The latter scheme has been successfully used to probe electron wave packet dynamics in atoms [21], and its acceleration (*streaking*) by intense infrared (IR) fields [22]. However, SAPs have broad spectral bandwidths that populate a large number of states and, consequently, they are not very selective. An alternative are attosecond pulse trains (APT), formed by consecutive attosecond pulses. APT are typically created from high harmonic generation, and they combine two advantages. First, they are easier to produce experimentally. Second, their spectral selectivity is much higher: the energy spectrum of an APT is not a broad distribution around the frequency of the pulse, such as in a SAP, but a series of spikes at odd multiples of the generating laser frequency. Therefore, the number of populated states is greatly reduced with respect to the SAP. Such APT-pump–IR-probe schemes have recently been used to study IR-assisted ionization of atoms [23,24], as well as to induce reconstruction of attosecond beatings by interference of two-photon transitions (RABITT) in H_2 photoionization [25].

However, a systematic study of the dynamics of autoionization in H_2 is still to be done. In this work we use a pump-probe scheme to study the dynamics of the Q_1 doubly excited states of the H_2 molecule with $^1\Sigma_u^+$ symmetry. The pump field is an APT whose most intense harmonic is tuned with the energy difference between the ground state of the molecule and the first Q_1 $^1\Sigma_u^+$ resonant state. The probe is a near-IR pulse used to track the autoionization dynamics. Both fields are linearly polarized in the direction of the internuclear axis. In our spectral method we can subtract any state we want from the calculations, so in order to study the effect of the Q_1 $^1\Sigma_u^+$ resonances, we compare the results for both the full calculation and one in which we have removed those states in the calculation. We also split the results into different final symmetries.

The paper is organized as follows. In Sec. II we describe in detail the theoretical method. Results are shown in Sec. III, focusing on photoelectron-photoion coincidence spectra (Sec. III A), photoelectron spectra (Sec. III B), and

*paula.riviere@uam.es

proton kinetic energy release spectra (Sec. III C). Finally, some conclusions are drawn in Sec. IV. Atomic units are used throughout unless otherwise specified.

II. THEORETICAL FRAMEWORK

Since the method has been explained in detail in Refs. [14–16], here we briefly summarize the basic ingredients. We solve the time-dependent Schrödinger equation (TDSE)

$$\left[\hat{H}_0(\mathbf{r}, R) + \hat{V}(t) - i \frac{\partial}{\partial t} \right] \Phi(\mathbf{r}, R, t) = 0, \quad (1)$$

where \mathbf{r} represents the electronic coordinates \mathbf{r}_1 and \mathbf{r}_2 , and R is the internuclear distance. \hat{H}_0 is the field-free nonrelativistic Hamiltonian of the H_2 molecule,

$$\hat{H}_0(\mathbf{r}, R) = \hat{T}(R) + \hat{H}_{\text{el}}(\mathbf{r}, R), \quad (2)$$

where $\hat{T}(R) = -\hat{\nabla}_R^2/2\mu$ is the relative kinetic energy of the nuclei, μ is the reduced mass, and $\hat{H}_{\text{el}}(\mathbf{r}, R)$ is the electronic Hamiltonian which includes the $1/R$ repulsion term. We neglect mass polarization terms, relativistic effects, and nonadiabatic couplings.

To deal with autoionization, we use the Feshbach formalism [18]. In this framework, we define two orthogonal complementary subspaces P and $Q = 1 - P$, with associated projectors \hat{P} and \hat{Q} , and expand the total wave function $\Phi(\mathbf{r}, R, t)$ in the basis of molecular eigenstates associated with each subspace. Since these states are not eigenstates of the molecular Hamiltonian, they will be coupled in the TDSE. More specifically, the time-dependent wave function $\Phi(\mathbf{r}, R, t)$ is expanded in a basis of vibronic stationary states, which are written as products of an electronic wave function and a vibrational or dissociative wave function [26]. The expansion includes three kinds of electronic wave functions, namely bound states, resonant states, and continuum states, calculated in a dense enough grid of internuclear distances [15]. The two former are obtained from configuration interaction calculations, while the latter is obtained from L^2 close-coupling calculations performed within a box [27,28].

The bound states Φ_n of the H_2 molecule are eigenfunctions of the electronic Hamiltonian,

$$\hat{H}_{\text{el}}(\mathbf{r}, R) \Phi_n(\mathbf{r}) = \mathcal{E}_n(R) \Phi_n(\mathbf{r}), \quad (3)$$

with eigenenergy \mathcal{E}_n . The resonances associated with the Q subspace are eigenfunctions of the projected Hamiltonian in Q subspace,

$$[\hat{Q} \hat{H}_{\text{el}} \hat{Q} - \mathcal{E}_r(R)] \Psi_r(\mathbf{r}; R) = 0 \quad (4)$$

and the nonresonant states associated with the electronic continuum in the P subspace are the solutions of the projected Schrödinger equation,

$$[\hat{P} \hat{H}_{\text{el}} \hat{P} - \mathcal{E}(R)] \Psi_\alpha^{\varepsilon l}(\mathbf{r}; R) = 0, \quad (5)$$

$$\mathcal{E}(R) - E_\alpha(R) + \varepsilon = 0. \quad (6)$$

Here α denotes the full set of quantum numbers for the electronic state of the molecular ion H_2^+ with a Born-Oppenheimer energy $E_\alpha(R)$, and ε and l are the energy and angular momentum of the ejected electron.

Once the electronic structure has been obtained in a given grid of internuclear distances, we solve the nuclear one-dimensional Schrödinger equation,

$$\left[-\frac{\nabla_R^2}{2\mu} + \mathcal{E}_x(R) \right] \chi_{v_x}(R) = W_{v_x} \chi_{v_x}(R), \quad (7)$$

where x stands for a bound, continuum, or resonant state of H_2 , and W_{v_x} is the vibronic energy associated with the x electronic state. The total wave function is thus written

$$\begin{aligned} \Phi(\mathbf{r}, R, t) = & \sum_n \sum_{v_n} C_{nv_n}(t) \Psi_n(\mathbf{r}; R) \chi_{v_n}(R) e^{-iW_{v_n}t} \\ & + \sum_r \sum_{v_r} C_{rv_r}(t) \Psi_r(\mathbf{r}; R) \chi_{v_r}(R) e^{-iW_{v_r}t} \\ & + \sum_{\alpha, l} \int d\varepsilon \sum_{v_\alpha} C_{\alpha, v_\alpha}^{\varepsilon l}(t) \Psi_\alpha^{\varepsilon l}(\mathbf{r}; R) \chi_{v_\alpha}(R) e^{-iW_{v_\alpha}t}, \end{aligned} \quad (8)$$

where the three terms represent the bound states, the resonant states, and the continuum states, respectively. Inserting Eq. (8) in Eq. (1) and projecting onto the basis of vibronic states leads to a set of coupled differential equations where the states with different symmetry are coupled by the laser potential, and the continuum and resonant states with the same symmetry are coupled by $\hat{Q} \hat{H}_{\text{el}} \hat{P}$ and $\hat{P} \hat{H}_{\text{el}} \hat{Q}$ terms. The TDSE is then integrated up to $t_{\text{max}} \gg T_{\text{AI}}$, where $T_{\text{AI}} = 1/\Gamma$ is the maximum autoionization time (corresponding to the minimum autoionization width Γ of all populated DES). The $\Psi_{kv_k}(\mathbf{r}, R)$ basis states are eigenstates of the field-free Hamiltonian at $t = \infty$, so the projection of the total wave function onto these states provides amplitudes that can be written in terms of the C_i expansion coefficients.

The interaction potential between the laser field and the H_2 molecule, $\hat{V}(t)$, is obtained within the dipole approximation, and using the velocity gauge it can be expressed as

$$\hat{V}(t) = (\hat{\mathbf{p}}_1 + \hat{\mathbf{p}}_2) \cdot \hat{\mathbf{A}}(t), \quad (9)$$

where $\hat{\mathbf{p}}_i$ is the momentum operator of electron i and $\hat{\mathbf{A}}(t)$ is the operator of the vector potential of the electromagnetic field, which is described classically.

To study the $Q_1^1 \Sigma_u^+$ resonances, we use an APT-pump-IR-probe setup, with linearly polarized light whose polarization direction is parallel to the internuclear axis. Thus only states of Σ_g^+ and Σ_u^+ symmetry will be populated. The APT is formed by a train of four xuv pulses with FWHM = 200 as and frequency 17ω , where $\omega = 1.605$ eV is the frequency of the generating IR field. The delay between the pulses in the train is $T/2$, where T is the IR period, which leads to an energy spectrum formed by odd harmonics of the generating frequency. This originates an energy spectrum with two principal harmonics at frequencies 17ω and 19ω (see Fig. 1), that we will denote H17 and H19, and the less intense harmonics H13, H15, H21, and H23. As can be seen in the figure, all parameters are chosen such that the $Q_1^1 \Sigma_u^+$ series of DESs is significantly populated. The intensity is 10^9 W/cm² for the two central pulses and 0.35×10^9 W/cm² for the external pulses, which corresponds to an APT envelope with FWHM = 3 fs and $I = 1.14 \times 10^9$ W/cm². The IR probe ($\omega = 1.605$ eV), which can also be used to generate the above

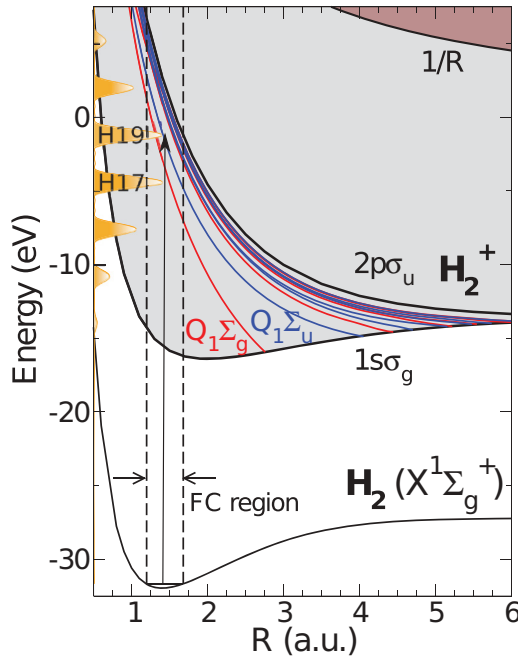


FIG. 1. (Color online) Born-Oppenheimer potential energy curves of the H₂ and H₂⁺ molecules. The energy spectrum of the APT is depicted in orange. The gray zone corresponds to ionization, and the Franck-Condon region lies between the vertical dashed lines. The black vertical arrow represents a vertical transition from the H₂ ground state to the lowest Q₁¹Σ_u⁺ resonance at the H₂ equilibrium distance ($R = 1.4$ a.u.).

APT, is three cycles long, has a sinus-square envelope, and an intensity of 10^{12} W/cm². To probe the dynamics of the resonant state, we perform a scan in delays between the APT pump and the IR probe. The delay Δt is defined with respect to the center of their corresponding envelopes, and $\Delta t > 0$ means that the xuv APT comes before the IR pulse. For $\Delta t = 0$, the xuv pulses are located at maxima and minima of the IR field.

The Born-Oppenheimer curves for the H₂ molecule are shown in Fig. 1, together with the APT spectrum. The figure shows the H₂ ground state and the two first electronic states of the H₂⁺ ion, $1\sigma_g$ and $2p\sigma_u$. The first series of resonances, Q₁, is shown for both the Σ_g⁺ (in red) and Σ_u⁺ (in blue) symmetries of the molecule. Note that all potential energy curves for the DES are repulsive, i.e., these resonant states can either dissociate on two neutrals, or decay into the H₂⁺ continuum.

Within the dipole approximation and for linearly polarized light, the selection rules impose that the total symmetry of the molecule changes parity after absorption of one photon. Therefore, if the initial state of the system is the ground rovibrational state of H₂, X¹Σ_g⁺, then the Q₁¹Σ_u⁺ states can be populated by one-photon absorption, but the Q₁¹Σ_g⁺ states only through absorption or emission of an even number of photons (e.g., one xuv photon plus one IR photon).

III. RESULTS

To study the dynamics of the Q₁¹Σ_u⁺ resonances, we will focus on the dissociative ionization process $H_2^{**} \rightarrow H + H^+ + e^-$. The observables will be the electron kinetic

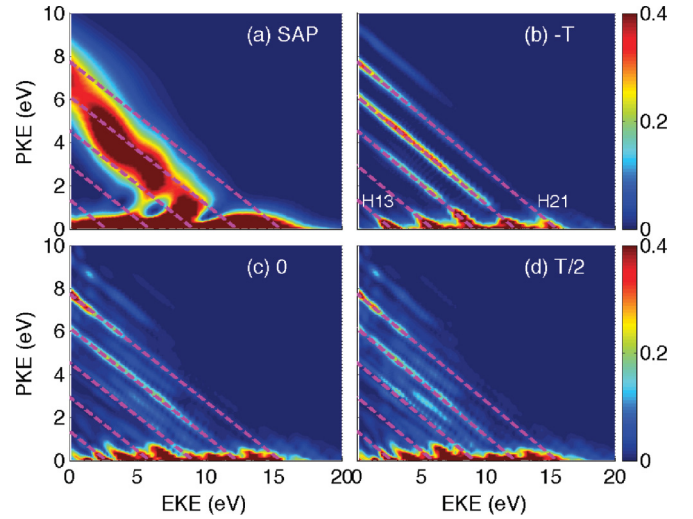


FIG. 2. (Color online) Doubly differential photoelectron-proton kinetic energy spectra for a SAP (a), and APT + IR at three different time delays: $\Delta t = -T$ (b), 0 (c), and $T/2$ (d), where T is the IR period. The dashed lines represent the energy conservation lines for the different harmonics (see text). The uppermost line corresponds to H21. All probabilities are multiplied by 10^6 .

energy (EKE) and the proton kinetic energy (PKE), either measured in coincidence or irrespective of each other. One of the advantages of using a spectral method is that we can select the states involved in the calculation as well as easily identify the final ionization channel. To unravel the role of the resonances we have performed three sets of calculations: with all states included, without the Q₁¹Σ_u⁺ states, and without the Q₁¹Σ_g⁺ states. Our calculations show that, in all cases, the effect of removing the ¹Σ_g⁺ resonances, which need at least two photons to be populated, is almost negligible. Therefore, we will mainly focus on the first two sets.

We note that H₂ single ionization leads predominantly to vibrationally bound states in the $1\sigma_g$ electronic state of the H₂⁺ molecular ion [$H_2 \rightarrow H_2^+(1\sigma_g, v) + e^-$]; see Fig. 1. Therefore, most electrons in the EKE distributions come from this nondissociative channel. Dissociative ionization is about two orders of magnitude smaller and is observed in both the $2p\sigma_u$ and $1\sigma_g$ channels. However, as Q₁¹Σ_u⁺ resonances mainly decay into the dissociative part of the ionization continuum, they will be more visible in the PKE spectrum than in the EKE one. An even more complete dynamical picture can be obtained by analyzing the two-dimensional (2D) coincidence photoelectron-proton kinetic energy spectrum. Autoionization of the Q₁¹Σ_u⁺ states will lead to either H₂⁺ in the $1\sigma_g$ state plus an ejected electron with odd angular momentum or to H₂⁺ in the $2p\sigma_u$ state plus an ejected electron with even angular momentum.

A. Doubly differential photoelectron-proton kinetic energy spectra

The calculated doubly differential photoelectron-proton kinetic energy spectra obtained by using the APT-pump-IR-probe scheme described in the previous section are shown in Fig. 2 for different time delays. For comparison, the figure also shows the results obtained with a SAP and no

IR pulse. This kind of representation, although difficult to achieve experimentally, contains very rich information on the photoionization dynamics, since it describes how energy is shared between electrons and nuclei (see, e.g., [29]). The dashed lines in the figure represent energy conservation for the different harmonic frequencies: for a given xuv-photon energy $\hbar\omega$, where ω is the xuv-photon frequency, the excess energy E^ω can be written as

$$E^\omega = \hbar\omega - (E_\infty - E_{v_0}) = \hbar\omega - 18.1 \text{ eV}, \quad (10)$$

where E_{v_0} is the energy of the ground rovibrational state of H_2 ($E_{v_0} = -31.7 \text{ eV}$) and E_∞ is the energy needed to reach the ionization threshold ($E_\infty = -13.6 \text{ eV}$). For example, for the harmonic H21 ($\hbar\omega = 33.6 \text{ eV}$), the excess energy is $E^{H21} = 15.5 \text{ eV}$. This harmonic corresponds to the uppermost dashed line in the figures: all possible energy sharings between the electron and the proton upon absorption of a H21 photon lay on the straight line that goes from $\text{EKE} = E^{H21}$ and zero PKE to zero EKE and $\text{PKE} = E^{H21}/2$.

In the result shown in Fig. 2(a) for a single attosecond pulse, one can see two well defined regions. The first one, in which probabilities are largest, corresponds to very slow protons, i.e., to electrons that take almost all the excess energy. This region reflects direct ionization through the $1s\sigma_g$ channel. The second region lies around the energy conservation lines, drawn in this case only for comparison, and corresponds to protons of intermediate energy. This region entirely reflects autoionization from the DESs that have been populated by the xuv photon. At the highest proton energies, part of the observed signal is due to direct photoionization through the $2p\sigma_u$ channel. This picture becomes much more complicated when we consider the APT + IR scheme, Figs. 2(b)–2(d), which we discuss next. When the IR pulse comes before the APT, [Fig. 2(b), delay $\Delta t = -T$], the 2D spectrum exclusively reflects the effect of the APT. This is because the IR pulse is not intense enough to induce a significant amount of ionization or electronic excitation in H_2 through multiphoton absorption. Thus, for all practical purposes, when the xuv APT arrives, the H_2 molecule is still in its ground state. After absorption of the xuv photons, a substantial part of the excess energy goes again to the electrons and leads to the pronounced signal at low proton energies. Nevertheless, this signal exhibits clear structures that follow the energy conservation lines that represent the expected final energies upon ionization by the harmonics from E^{H21} (uppermost line) down to E^{H13} . Along these energy conservation lines and for intermediate proton energies, the ionization probability is also high, which is entirely due to autoionization of the DESs that have been populated by the xuv photon. Besides, at the highest proton energies and very small EKE, there is the signature of direct photoionization into the $2p\sigma_u$ continuum. So, the 2D spectrum of Fig. 2(b) reflects exactly the same features as those of Fig. 2(a) for the SAP, but only along the energy conservation lines that correspond to the different harmonic energies.

When the APT and IR fields overlap, the APT drives first the system into the continuum whence absorption or emission of few IR photons is now possible. The latter processes lead to final energies right in the middle between the harmonic bands. The resulting sidebands are clearly visible for $\Delta t = 0$ (c) and $T/2$ (d). The dynamics of the autoionization

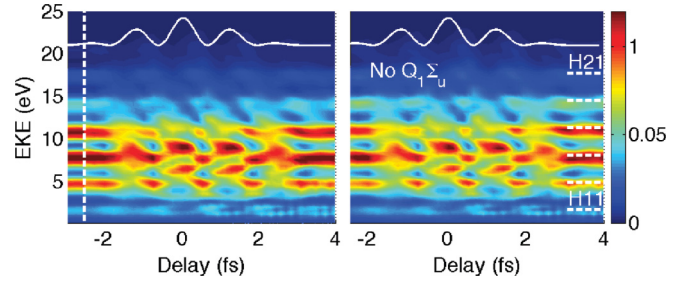


FIG. 3. (Color online) Photoelectron spectrum for the full calculation (left) and without $Q_1^1 \Sigma_u^+$ resonances (right). Results without IR field (only APT) are shown at the left of the white vertical line. The expected final energy upon absorption of a photon from each harmonic order is shown with horizontal lines. The square of the vector potential is shown in the upper part of the figures. All probabilities are multiplied by 10^6 .

process can be easily followed by analyzing the variation of the 2D spectrum with time delay [see the movie given in the Supplemental Material [30], from which the snapshots shown in Figs. 2(b)–2(d) have been extracted]. Indeed, as mentioned above, DESs have repulsive energy curves (see Fig. 1). Therefore, when one of these states is populated by an xuv photon, the molecule starts to increase its internuclear distance, and it can either lead to dissociation into two neutral atoms or decay into the ionization continuum. The longer the molecule has evolved in the dissociating curve, the higher will be the kinetic energy gained by the nuclei. Consequently, the higher the proton energy in a given energy-conservation line, the larger the autoionization lifetime of the DES.

Although these 2D PKE-EKE spectra are very useful to understand the photoionization process, it is much more feasible experimentally to obtain integrated photoelectron and proton kinetic energy spectra. We show results for both in the next two subsections.

B. Photoelectron spectra

The photoelectron spectrum as a function of time delay is shown in Fig. 3 both for the full calculation (left) and the calculation without the $Q_1^1 \Sigma_u^+$ resonances (right). The results of a calculation in which only the APT was used (i.e., no IR pulse) is shown at the left of the vertical dashed line in the left panels. The square of the vector potential is shown at the top of the figures. The horizontal lines on the right of the photoelectron spectra indicate, for the different harmonic energies, the energy available for the electron when the system is in the $v = 2$ vibrational level of the $1s\sigma_g$ state of the H_2^+ ion (with $v = 3$, they have the highest population for all delays). Since higher vibrational levels are also populated (corresponding to lower kinetic electron energies), these lines serve as an upper bound for the electron energy corresponding to photon absorption from each of the harmonics.

As expected, the EKE spectra with and without the $Q_1^1 \Sigma_u^+$ resonances are almost identical because the dominant process is nondissociative direct ionization. The bands corresponding to the different harmonics are clearly visible. When there is no IR, only the bands corresponding to the odd harmonics are present. For negative delays (IR pulse before the xuv APT),

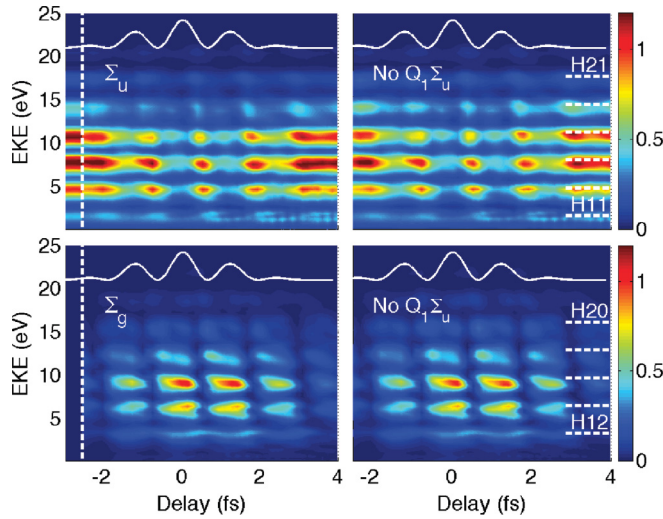


FIG. 4. (Color online) Same as in Fig. 3, but split into total symmetry Σ_u (top figures) and Σ_g (bottom figures).

the EKE is almost identical to that without the IR because, as mentioned above, the IR intensity is not high enough to induce photoionization or significant electronic excitation, so that when the APT arrives the H₂ molecule is mostly in its ground state. When both fields overlap ($\Delta t \sim 0$), the molecule is first ionized by an xuv photon and then it can either absorb or emit IR photons, leading to the formation of sidebands located at even harmonics of the generating frequency. For positive delays, the xuv comes first and the resulting molecular ion evolves in time until the IR photon is absorbed. The resulting bands and sidebands vary with the time delay with a period $T/2$. This periodicity has already been observed [23] and explained [31,32] in atomic systems when similar setups have been used. It has also been recently observed in the H₂ molecule [25]. When $\Delta t \gg \text{FWHM}$ there is no more overlap between the pulses: the molecule absorbs an xuv photon and the ejected electron is not affected by the IR field, so the EKE is again maximum at odd harmonics.

In order to understand the dynamics of this process we can split the EKE spectra into contributions from different symmetries: Σ_u and Σ_g . This is shown in Fig. 4: the top two figures show the dissociative ionization probabilities for the Σ_u symmetry, which can be directly accessed by absorption of a single xuv photon (i.e., the odd harmonic bands), and the bottom two figures those for the Σ_g symmetry, which need the emission or absorption of at least one IR photon (i.e., the sidebands). The latter are only significantly populated when both pulses overlap. Note that for each symmetry there is a clear pattern with $T/2$ periodicity. When the transition probability to the sidebands (bottom) is maximized, there is a depletion in the odd harmonic bands (top). This occurs when the combined absorption of an xuv and an IR photon is efficient, i.e., when the attosecond pulses of the APT lie around the maxima of the IR field. The combination of these two clear patterns produces the complicated spectrum in Fig. 3.

Apart from the expected broadening of the different bands and sidebands due to the sharing of the excess energies between the ejected electron and the nuclear vibrational states of the final H₂⁺ molecular ion, these results are not substantially

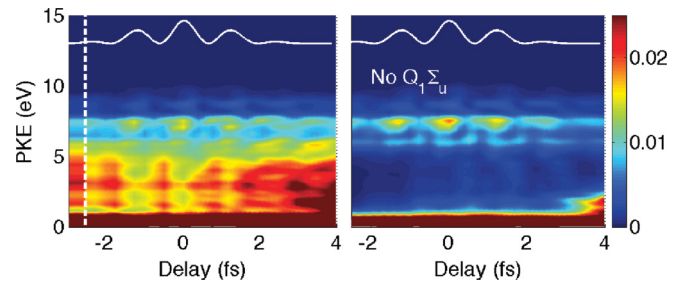


FIG. 5. (Color online) Proton kinetic energy spectrum for the full calculation (left) and without $Q_1^1 \Sigma_u^+$ resonances (right). Results without IR field (only APT) are shown at the left of the white vertical line. The square of the vector potential is shown in the upper part of the figures. All probabilities are multiplied by 10^6 .

different from those already found in atoms [33,34]. This is simply because the EKE spectra are entirely dominated by direct ionization without a significant dissociation of the remaining molecular ion.

C. Proton kinetic energy spectra

The PKE spectra resulting from both the full calculation (left) and that without the $Q_1^1 \Sigma_u^+$ resonances (right) are shown in Fig. 5 as a function of time delay. Both figures show an intense band of low proton energy (< 1 eV), which corresponds to direct dissociative ionization through the $1s\sigma_g$ channel. There is also a faint contribution at proton energies $E \sim 7.75$ eV, which corresponds to direct dissociative ionization through the $2p\sigma_u$ channel. This channel is open within the Franck-Condon region for the harmonic H21. For $\Delta t > 3.5$ fs, the low energy band widens, which is the signature of bond softening: the nuclear wave packet launched by the xuv field in the $1s\sigma_g$ state evolves to higher internuclear distances, where the $2p\sigma_u$ state is much closer in energy and it is therefore accessible after absorption of a few IR photons. This effect has been previously observed in H₂ by using a SAP-pump-IR-probe scheme [20]. The signal associated with autoionization from the DESs is clear in the results of the

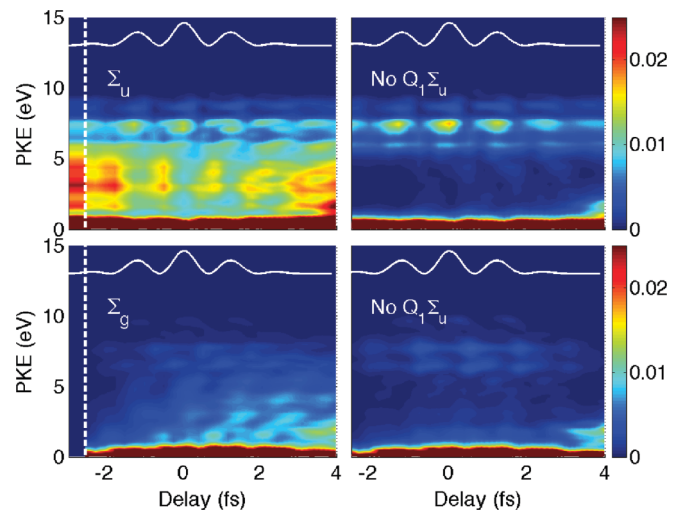


FIG. 6. (Color online) Same as in Fig. 5, but split into total symmetry Σ_u (top figures) and Σ_g (bottom figures).

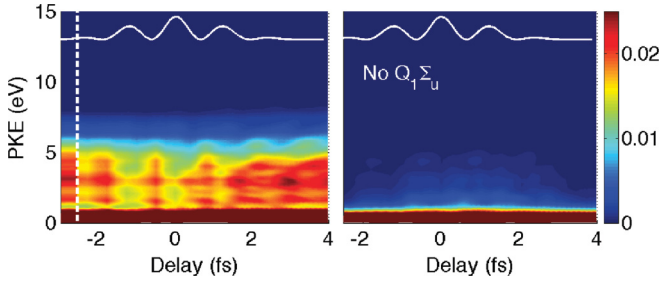


FIG. 7. (Color online) Same as in Fig. 5, but including only the $1s\sigma_g$ continuum.

full calculation (Fig. 5, left): it appears at intermediate proton energies (1–6 eV) with $T/2$ periodicity and disappears when the $Q_1 \ ^1\Sigma_u^+$ states are removed from the calculations (Fig. 5, right).

The Σ_u and Σ_g contributions to the above spectra are shown in Fig. 6. In the full calculation for the Σ_u symmetry, one can clearly see autoionization from the $Q_1 \ ^1\Sigma_u^+$ DESs to the continuum of the same symmetry at intermediate proton energies, while this process is totally absent when the $Q_1 \ ^1\Sigma_u^+$ states are removed from the calculations. In the Σ_g symmetry, one can also observe a faint contribution from these resonances at intermediate proton energies resulting from the radiative decay of the $Q_1 \ ^1\Sigma_u^+$ DESs to the $1s\sigma_g(\Sigma_g)$ continuum upon absorption or emission of an IR photon; see Fig. 1.

The signature of autoionization can be seen even more clearly if we remove the contribution of the $2p\sigma_u$ continuum from the PKE. The result is shown in Fig. 7, that should be compared with Fig. 5: when the $2p\sigma_u$ contribution is removed, both the band at high energies and the bond softening at long delays disappear, and only the resonances remain.

IV. CONCLUSIONS

In this work we have studied the autoionization dynamics of the first series of doubly excited states of the H_2 molecule, the $Q_1 \ ^1\Sigma_u^+$ series, by using an APT-pump-IR-probe scheme in which the xuv photons of the APT are used to populate the doubly excited states and the dynamics is tracked by changing the delay between the APT pump and the IR probe. For this, we have solved the time-dependent Schrödinger equation by using a close-coupling method that accounts for all vibrational and

electronic degrees of freedom of the molecule. To simplify the analysis and the calculations, the case of H_2 molecules oriented parallel to the polarization direction has been considered.

We did three series of calculations: with all Q_1 resonances, without the $Q_1 \ ^1\Sigma_u^+$ states, and without the $Q_1 \ ^1\Sigma_g^+$ states. The last set of calculations leads to results that are almost identical to those from the full calculation, showing that by using this pump-probe scheme, the population of the optically forbidden Σ_g^+ resonances is negligible. Our spectral method also allows us to analyze separately the contribution of the Σ_g^+ and Σ_u^+ final symmetries.

We have shown results for doubly differential photoelectron-proton kinetic energy spectra (or 2D coincidence spectra, for simplicity) in the case of a SAP, as well as for the APT + IR scheme at different time delays. The autoionization dynamics can be easily followed by looking at the variation of the 2D spectrum with time delay. We have also shown results for the integrated electron kinetic energy (EKE) and proton kinetic energy (PKE) spectra. In the EKE spectrum, we observe a complicated pattern that can be easily understood by analyzing the Σ_g^+ and Σ_u^+ contributions separately. Autoionization leaves almost no trace in the EKE spectrum, but it plays a dominant role in PKE spectrum since it is responsible for almost all the protons ejected in the 1–6 eV energy region.

In summary, APT-pump-IR-probe schemes are a useful tool to track autoionization dynamics in molecules. An alternative setup, such as (APT + IR)-pump-IR-probe, would be necessary to probe doubly excited states of $^1\Sigma_g^+$ symmetry.

ACKNOWLEDGMENTS

This work was accomplished with an allocation of computer time from Mare Nostrum BSC and CCC-UAM, and was partially supported by the MICINN Projects No. FIS2010-15127, No. ACI2008-0777, and No. CSD 2007-00010, the ERA-Chemistry Project No. PIM2010EEC-00751, the European grants MC-ITN CORINF and MC-RG ATTOTREND, the European COST Action CM0702, and the Advanced Grant of the European Research Council XCHEM 290853. R.E.F.S. acknowledges a Ph.D. contract from ITN CORINF. P.R. acknowledges a Juan de la Cierva contract grant from MICINN.

-
- [1] J. Ullrich, R. Moshhammer, R. Dörner, O. Jagutzki, V. Mergel, H. Schmidt-Böcking, and L. Spielberger, *J. Phys. B: At. Mol. Opt. Phys.* **30**, 2917 (1997).
 - [2] T. Jahnke, T. Weber, A. Landers, A. Knapp, S. Schössler, J. Nickles, S. Kammer, O. Jagutzki, L. Schmidt, A. Czasch *et al.*, *Phys. Rev. Lett.* **88**, 073002 (2002).
 - [3] A. Lafosse, M. Lebech, J. C. Brenot, P. M. Guyon, L. Spielberger, O. Jagutzki, J. C. Houver, and D. Doweck, *J. Phys. B: At. Mol. Opt. Phys.* **36**, 4683 (2003).
 - [4] T. Jahnke, L. Foucar, J. Titze, R. Wallauer, T. Osipov, E. Benis, A. Alnaser, O. Jagutzki, W. Arnold, S. Semenov *et al.*, *Phys. Rev. Lett.* **93**, 083002 (2004).
 - [5] J. Ullrich, R. Moshhammer, R. Dörner, R. Dörner, L. P. H. Schmidt, and H. Schmidt-Böcking, *Rep. Prog. Phys.* **66**, 1463 (2003).
 - [6] F. Martín, J. Fernández, T. Havermeier, L. Foucar, T. Weber, K. Kreidi, M. Schöffler, L. Schmidt, T. Jahnke, O. Jagutzki *et al.*, *Science* **315**, 629 (2007).
 - [7] M. S. Schöffler, J. Titze, N. Petridis, T. Jahnke, K. Cole, L. P. H. Schmidt, A. Czasch, D. Akoury, O. Jagutzki, J. B. Williams *et al.*, *Science* **320**, 920 (2008).
 - [8] B. Zimmermann, D. Rolles, B. Langer, R. Hentges, M. Braune, S. Cvejanovic, O. Geszner, F. Heiser, S. Korica, T. Lischke *et al.*, *Nature Phys.* **4**, 649 (2008).

- [9] M. Drescher, M. Hentschel, R. Kienberger, M. Uiberacker, V. Yakovlev, A. Scrinzi, T. Westerwalbesloh, U. Kleineberg, U. Heinzmann, and F. Krausz, *Nature (London)* **419**, 803 (2002).
- [10] L. Miaja-Avila, G. Saathoff, S. Mathias, J. Yin, C. La-o-vorakiat, M. Bauer, M. Aeschlimann, M. M. Murnane, and H. C. Kapteyn, *Phys. Rev. Lett.* **101**, 046101 (2008).
- [11] X. M. Tong, P. Ranitovic, C. W. Hogle, M. M. Murnane, H. C. Kapteyn, and N. Tushima, *Phys. Rev. A* **84**, 013405 (2011).
- [12] P. Ranitovic, X. M. Tong, C. W. Hogle, X. Zhou, Y. Liu, N. Tushima, M. M. Murnane, and H. C. Kapteyn, *Phys. Rev. Lett.* **106**, 053002 (2011).
- [13] S. Zharebtsov, A. Wirth, T. Uphues, I. Znakovskaya, O. Herrwerth, J. Gagnon, M. Korbman, V. S. Yakovlev, M. J. J. Vrakking, M. Drescher *et al.*, *J. Phys. B: At. Mol. Opt. Phys.* **44**, 105601 (2011).
- [14] A. Palacios, H. Bachau, and F. Martín, *Phys. Rev. Lett.* **96**, 143001 (2006).
- [15] J. L. Sanz-Vicario, H. Bachau, and F. Martín, *Phys. Rev. A* **73**, 033410 (2006).
- [16] A. Palacios, H. Bachau, and F. Martín, *Phys. Rev. A* **75**, 013408 (2007).
- [17] U. Fano, *Phys. Rev.* **124**, 1866 (1961).
- [18] H. Feshbach, *Ann. Phys. (NY)* **19**, 287 (1962).
- [19] J. F. Pérez-Torres, F. Morales, J. L. Sanz-Vicario, and F. Martín, *Phys. Rev. A* **80**, 011402(R) (2009).
- [20] G. Sansone, F. Kelkensberg, J. F. Pérez-Torres, F. Morales, M. F. Kling, W. Siu, O. Ghafur, P. Johnsson, M. Swoboda, E. Benedetti *et al.*, *Nature (London)* **465**, 763 (2010).
- [21] J. Mauritsson, T. Remetter, M. Swoboda, K. Klünder, A. L'Huillier, K. J. Schafer, O. Ghafur, F. Kelkensberg, W. Siu, P. Johnsson *et al.*, *Phys. Rev. Lett.* **105**, 053001 (2010).
- [22] R. Kienberger, E. Goulielmakis, M. Uiberacker, A. Baltuska, V. Yakovlev, F. Bammer, A. Scrinzi, T. Westerwalbesloh, U. Kleineberg, U. Heinzmann *et al.*, *Nature (London)* **427**, 817 (2004).
- [23] P. Johnsson, J. Mauritsson, T. Remetter, A. L'Huillier, and K. J. Schafer, *Phys. Rev. Lett.* **99**, 233001 (2007).
- [24] P. Ranitovic, X. M. Tong, B. Gramkow, S. De, B. DePaola, K. P. Singh, W. Cao, M. Magrakvelidze, D. Ray, I. a. Bocharova *et al.*, *New J. Phys.* **12**, 013008 (2010).
- [25] F. Kelkensberg, W. Siu, J. F. Pérez-Torres, F. Morales, G. Gademann, A. Rouzée, P. Johnsson, M. Lucchini, F. Calegari, J. L. Sanz-Vicario *et al.*, *Phys. Rev. Lett.* **107**, 043002 (2011).
- [26] A. Palacios, H. Bachau, and F. Martín, *Phys. Rev. A* **74**, 031402(R) (2006).
- [27] F. Martín, *J. Phys. B: At. Mol. Opt. Phys.* **32**, 197R (1999).
- [28] H. Bachau, E. Cormier, P. Decleva, J. P. Hansen, and F. Martín, *Rep. Prog. Phys.* **64**, 1815 (2001).
- [29] A. González-Castrillo, A. Palacios, F. Catoire, H. Bachau, and F. Martín, *J. Phys. Chem. A* **116**, 2704 (2012).
- [30] See Supplemental Material at <http://link.aps.org/supplemental/10.1103/PhysRevA.85.063414> for doubly differential photoelectron-proton kinetic energy spectra for an APT + IR combined field as a function of the time delay between them, indicated in the legend. The dashed lines represent the energy conservation lines for the different harmonics. The uppermost line corresponds to H21. All probabilities are multiplied by 10⁶; The second movie shows the same as before, but when the Q₁¹Σ_u⁺ resonances are removed from the calculations.
- [31] P. Rivière, O. Uhden, U. Saalmann, and J. Rost, *New J. Phys.* **11**, 053011 (2009).
- [32] X. M. Tong, P. Ranitovic, C. L. Cocke, and N. Tushima, *Phys. Rev. A* **81**, 021404(R) (2010).
- [33] F. Quéré, Y. Mairesse, and J. Itatani, *J. Mod. Opt.* **52**, 339 (2005).
- [34] K. Klünder, J. Dahlström, M. Gisselbrecht, T. Fordell, M. Swoboda, D. Guénot, P. Johnsson, J. Caillat, J. Mauritsson, A. Maquet *et al.*, *Phys. Rev. Lett.* **106**, 143002 (2011).